Proton-Proton Scattering Experiments at 170 and 260 Mev*

OWEN CHAMBERLAIN AND JOHN D. GARRISON†
Radiation Laboratory and Department of Physics, University of California, Berkeley, California
(Received April 2, 1956)

The differential proton-proton scattering cross section has been measured at 170 and 260 Mev for laboratory angles of 4.4° to 30°. The proton beam was obtained by reducing the energy of the 345-Mev beam of Berkeley cyclotron. A liquid-hydrogen target was used. Counting was done with a telescope of two liquid scintillation counters. A Faraday cup served as a standard for beam calibration.

The results indicate a cross section, in the center-of-mass system, independent of energy, and rather independent of angle, outside of the Coulomb region. The level of the differential cross section is close to 3.6 millibarns per steradian. An approximate treatment indicates there is destructive interference between nuclear and Coulomb scattering. It is concluded that the real part of the nuclear scattering amplitude must be positive at small angles.

I. INTRODUCTION

EXPERIMENTS on *p-p* and *n-p* scattering have been performed from very low energies to energies in the Bev region.[1] The nucleon-nucleon scattering data up to about 10 Mev seem quite complete and subject to unambiguous analysis, as summarized by Jackson and Blatt.[2] At high energies, above the 400-Mev range, the experimental information is quite incomplete, and in addition, meson production and relativistic effects are sufficiently large that no exact analysis has been possible. In the intermediate range of energies, in which this experiment was performed, the analysis is complicated, owing principally to the importance of the higher angular-momentum states. In this energy region, if the view is taken that the experimental work is incomplete until the phase shifts involved are determined, it is clear that a great deal more work remains to be done. In fact, scattering experiments of the type described in this paper, in which both target and beam are unpolarized, are insufficient to determine all the phase shifts, since there are many combinations of phase shifts that yield agreement with the observed scattering. Before a complete determination of the phase shifts is possible, experiments using polarized beams and also triple-scattering experiments must be taken into account.[3]

In earlier work Chamberlain, Segrè, and Wiegand have conducted a series of *p-p* scattering experiments at this laboratory with proton energies of 120 to 345 Mev.[4] With reduced proton energies, other than 345 Mev, they were unable to complete the differential cross-section measurements at angles close to the cyclotron beam because of the large counter background that arose in the process of reducing the beam energy. This paper extends these reduced-energy scattering results to the smaller angles. Measurements have been made at laboratory angles of 4.4° to 30°. It is in this angular region that various potential models have been at greatest variance with the measured *p-p* cross section at these energies.[5]

In this experiment the counting method is somewhat different from that previously employed, in that considerable absorber was placed in the counter telescope when measurements were made at small angles to the beam. Furthermore, the counting rates with the liquid-hydrogen target and dummy target were determined with slightly different absorber thicknesses, to compensate for the liquid-hydrogen stopping power. This method has proved quite important in eliminating background at small angles.

Results will be found in Tables III and IV and Figs. 11 and 12.

II. EXPERIMENTAL METHOD

In order to obtain data in the small-angle region, a number of changes in the techniques previously used were found necessary. The target protons were in the form of liquid hydrogen, replacing the CH_2-C difference method used at wider angles.[6] The construction of

* This work was done under the auspices of the U. S. Atomic Energy Commission.

† Now at San Diego State College, San Diego, California.

[1] A summary of the earlier work is contained in an article by R. S. Christian, Repts. Progr. in Phys. **15**, 68 (1952). Some of the more recent papers are: Marshall, Marshall, and Nedzell, Phys. Rev. **92**, 834 (1953); Cassels, Pickavance, and Stafford, Proc. Roy. Soc. (London) **214**, 262 (1952); Kruse, Teem, and Ramsey, Phys. Rev. **94**, 1795 (1954); Sutton, Fields, Fox, Kane, Mott, and Stallwood, Phys. Rev. **97**, 783 (1955); Chamberlain, Pettengill, Segrè, and Wiegand, Phys. Rev. **93**, 1424 (1954); R. H. Stahl and N. F. Ramsey, Phys. Rev. **96**, 1310 (1954); A. J. Hartzler and R. T. Siegel, Phys. Rev. **95**, 185 (1954); D. Fischer and G. Goldhaber, Phys. Rev. **95**, 1350 (1954); O. Chamberlain and J. W. Easley, Phys. Rev. **94**, 208 (1954).

[2] J. D. Jackson and J. M. Blatt, Revs. Modern Phys. **22**, 77 (1950); Phys. Rev. **76**, 18 (1949).

[3] Considerable work with polarized proton beams has been done recently; for example: C. L. Oxley *et al.*, Phys. Rev. **91**, 419 (1953); Chamberlain, Segrè, Wiegand, Tripp, and Ypsilantis, Phys. Rev. **93**, 1430 (1954); Marshall, Marshall, and de Carvalho, Phys. Rev. **93**, 1431 (1954); Kane, Stallwood, Sutton, Fields, and Fox, Phys. Rev. **95**, 1694 (1954); Chamberlain, Donaldson, Segrè, Tripp, Wiegand, and Ypsilantis, Phys. Rev. **95**, 850 (1954); Ypsilantis, Wiegand, Tripp, Segrè, and Chamberlain, Phys. Rev. **98**, 840 (1955).

[4] Chamberlain, Segrè, and Wiegand, Phys. Rev. **83**, 923 (1951).

[5] A number of theoretical papers using potential models are given in the article by R. S. Christian cited in reference 1.

[6] The target is a modification of the one described by Leslie Cook, Rev. Sci. Instr. **22**, 1006 (1951). The modification is discussed by J. W. Mather and E. A. Martinelli, Phys. Rev. **92**, 780 (1953).

the liquid-hydrogen container is shown in Fig. 1. The 345-Mev proton beam from the cyclotron was reduced to the desired energy by passage through a beryllium absorber similar in function to the lithium absorber used by Chamberlian, Segrè, and Wiegand. The beam was subsequently collimated and analyzed in a magnetic field to regain a beam reasonably homogeneous in energy and free of neutrons. The 90°-coincidence counting method could not be used because of the low energy of one of the partner protons, and was replaced by a coincidence telescope, which viewed a single proton at the desired angle. It was thought desirable to measure the cross sections at just two energies because of the limited time available on the cyclotron. The energies selected were 170 and 260 Mev.

The experimental results given here were obtained during two 3-day cyclotron runs designated as Run No. 1 and Run No. 2. It seemed desirable to repeat the measurements of Run No. 1, as was done in improved form for Run No. 2, to check the consistency of the method. The data from Run No. 2 should be given slightly greater weight because of certain improvements in technique. Minor equipment changes were made between the two runs.

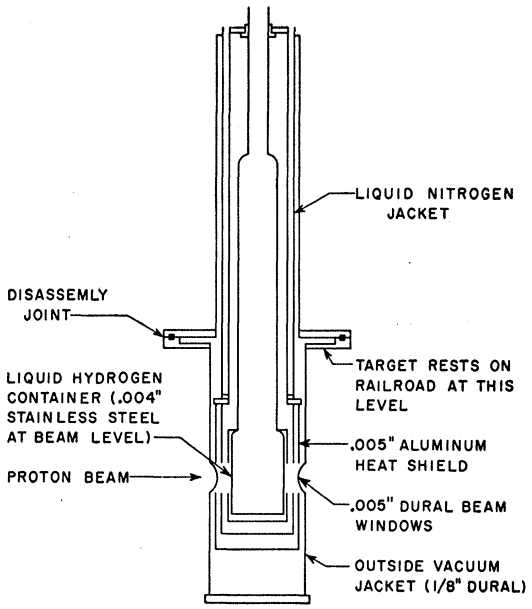

FIG. 1. Cross-sectional view of the liquid hydrogen target.

Cross-Section Equations

The number of hydrogen-scattered protons is related to the differential scattering cross sections in the laboratory system by the equation

$$H=nN\sigma(\Phi)\Omega, \tag{1}$$

where $\sigma(\Phi)$ is the laboratory differential cross section at angle Φ to the beam; Ω is the solid angle subtended by the defining counter, as seen from the point of scattering; H is the number of protons per unit beam scattered by hydrogen into the solid angle Ω; n is the number of beam protons per unit beam; and N is the number of target protons per square centimeter traversed by the beam.

The number of beam protons, n, has been measured with a parallel-plate ionization chamber with an argon atmosphere. Each beam proton passing through the ionization chamber produces many ion pairs in the argon gas, so that the current in the ionization chamber is greater than the beam current. The ratio of ionization current to beam current is denoted by M and is called the ionization-chamber multiplication. Current from the ionization chamber was used to charge a capacitance C. The potential difference across this capacitance was measured by an electrometer-and-recorder circuit. When the condenser C has been charged to a standard voltage V, unit beam is said to have passed through the ionization chamber. The number of protons per unit beam is thus $n=CV/eM$, in which e is the electronic charge.

In practice, an absorber has been inserted in the counter telescope in many of the measurements, for reasons to be described below. This absorber and also the counters and hydrogen containers have inevitably involved some loss of scattered particles—mainly those that collide with nuclei in the absorber. To correct for this loss an experimentally determined factor is required. This factor was combined with the multiplication factor in our calculations to yield M^*, the effective multiplication. M^* thus depends on angle of scattering and on absorber thickness, as well as on beam energy.

The number of target hydrogen atoms per square centimeter, N, is given simply in terms of the target length L traversed by the beam, the density ρ of liquid hydrogen, and the mass m of one hydrogen atom. The expression is

$$N=\rho L/m.$$

The solid angle Ω subtended by the counter at the target center is given in terms of the counter area A and the counter-to-target distance r, as

$$\Omega=A/r^2.$$

Equation (1) for the differential scattering cross section in the laboratory coordinate system may be rewritten in the form

$$\sigma(\Phi)=KM^*H, \tag{2a}$$

in which

$$K=er^2m/CVA\rho L. \tag{2b}$$

For conversion to the center-of-mass system, one has

$$\sigma(\theta)=[1+(E/2mc^2)\sin^2\Phi]^2 \times\sigma(\Phi)/[1+E/2mc^2]4\cos\Phi, \tag{3}$$

$$\tan(\theta/2)=[1+E/2mc^2]^{\frac{1}{2}}\tan\Phi, \tag{4}$$

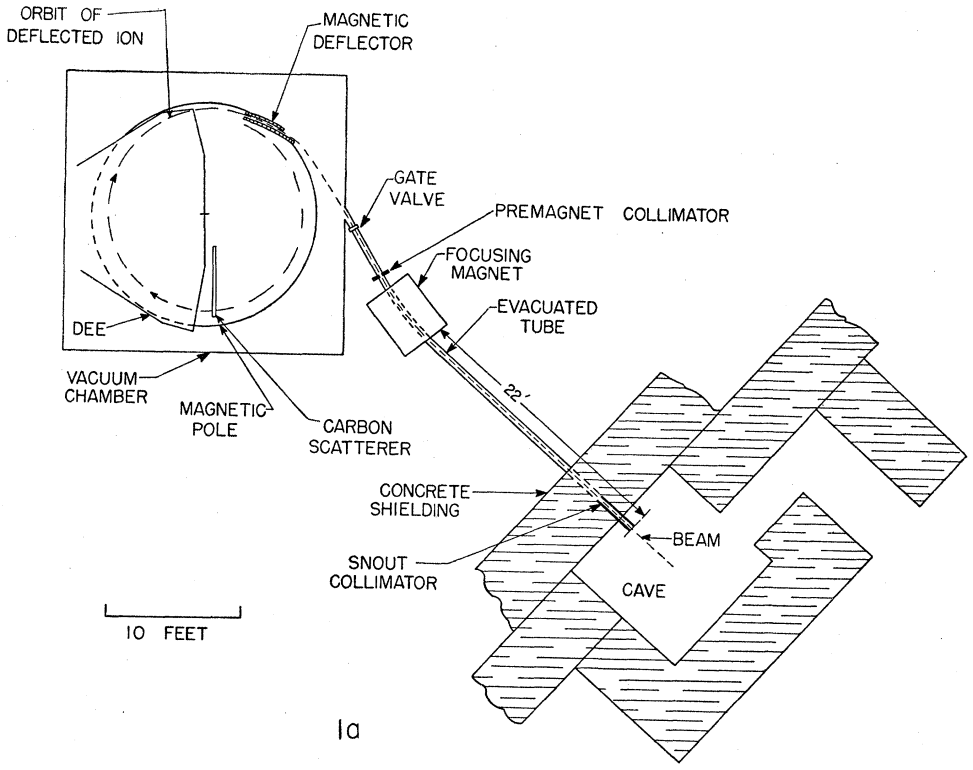

FIG. 2. The general arrangement of the experiment.

where $\sigma(\theta)$ is the center-of-mass differential scattering cross section at center-of-mass angle θ to the beam direction, E is the kinetic energy of the incident beam protons in the laboratory system, and mc^2 is the proton rest energy.

The remainder of this paper discusses the measurement of the quantities in Eqs. (2a), (2b), and (3).

The Cyclotron Beam

The "scattered" beam of the 184-inch Berkeley cyclotron emerges from the magnetic field of the cyclotron through a magnetic shielding tube, is deflected by the magnetic field of a focusing magnet, and then is brought out through the main concrete shielding of the cyclotron into the experimental area (Fig. 2). In traversing the concrete shielding, the beam is collimated by a cyclindrical brass collimator 46 inches in length and 0.5 inch in diameter, which, however, widens to 0.75 inch in diameter for the last 15 inches of its length. Following this collimator the beam goes through a 10-mil aluminum window in passing from the vacuum into the air.

TABLE I. Collimator slit dimensions (inches).

Collimator	Width	Height	Length
I	0.5	0.75	2.75
II	0.5	0.75	2.75
III	0.25	0.75	4
IV	0.375	0.75	2.75
V	0.5	1	2.75
VI	1.5	1.5	2.75

Beam pulses occur at the rate of 60 per second. Each beam pulse lasts over a period of 20 to 30 microseconds, but is modulated into short bursts at the radio-frequency of the cyclotron, 16 Mc/sec. The mean energy of this beam as it enters the cave is 345 Mev.

Energy-Reduction System

In the cave, following the 46-inch collimator, was the beam-energy-reduction system (Fig. 3). The collimator slit sizes are listed in Table I. The beam energy was reduced in beryllium absorbers 1 by 1.1 inches by a length suitable for the desired energy reduction. This length was slightly less than 12 inches for the 170-Mev beam. Considerable brass and lead shielding surrounded the system of absorbers.

A great deal of effort was spent in determing a best collimating and analyzing system. The approach is limited by the desire not to sacrifice beam intensity. Emphasis was placed on obtaining a beam as homogeneous in energy as possible and as free as possible from protons scattered by the collimator materials.

The reduced-energy beam was magnetically analyzed. The magnetic analysis was adopted as soon as it was determined that it would not involve prohibitive loss of beam intensity. It serves to eliminate lower energy protons originating in the beryllium absorber and the first few collimators. The latter make a major contribu-

tion because of the very considerable multiple scattering in the beryllium. Magnetic analysis also reduces any neutron background. In the reduction of the energy of the proton beam, the beam was attenuated by a factor of about 50 to 200, giving maximum proton currents of 10^{-13} and 3×10^{-14} ampere for the 260- and 170-Mev beams.

A series of slit collimators was used instead of a continuous collimator tube, to reduce the number of particles that continue in the beam after scattering from the collimators. The final series of slits was made with successively larger apertures so that the final slits would act only to eliminate particles scattered from the walls of previous slits. This feature was found indispensable for a reason that may be outlined as follows. Some particles may reach the counter telescope without scattering in hydrogen if they are scattered by material of one of the last slits in the collimator system. These protons will have lost some energy in the slit material, and in fact some of them will be of very low energy (and of correspondingly short residual range). They constitute a treacherous background that is very sensitive to the amount of absorber in their path. Even when a difference is taken between counting rates with the hydrogen target and the empty dummy target, this background will still not be fully corrected, since the background will have been altered by the stopping power of the liquid hydrogen. The most effective single factor in reducing the counting background arising in the collimating system was an antiscattering block placed on the

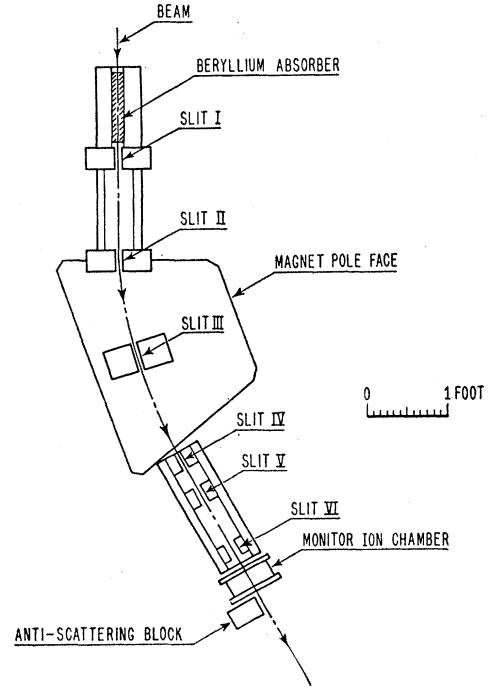

FIG. 3. The beam energy-reduction system. Roman numerals indicate the collimator slit numbers corresponding to Table I.

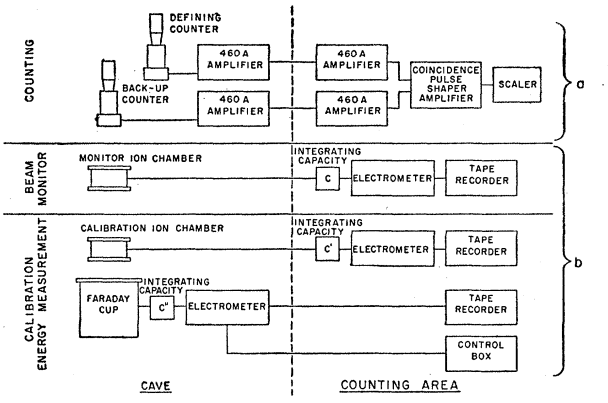

FIG. 4. Block diagram of the electronics used in the experiment.

counter-telescope side of the beam and preceding the hydrogen target, so that the telescope, at the smallest angle counted, could not see the next-to-last collimator slit.

The reduced beams at each energy traversed the same collimating system, while being bent through an angle of approximately 28° by the analyzing magnet. The magnetic field was about 14 000 gauss for the 260-Mev beam, and somewhat over 11 000 gauss for the 170-Mev beam. The energy resolution of the beam reduction system was 10%, as determined by the current-carrying-wire method of simulating the beam trajectory.

The Counting Electronics

The two counters used to form the counter telescope were liquid scintillators viewed by single 5819 photomultiplier tubes, with Lucite containers for the liquid and using Lucite light pipes following approximately the principle of Garwin.[7] It was thought that this type of counter would be better for coincidence counting because of its more uniform pulse heights, although no pulse-height measurements were attempted. To eliminate the effects of stray magnetic fields, the photomultiplier tubes were encased in $\frac{1}{4}$-inch-thick soft-iron pipes in addition to the mu-metal shields that accompanied the 5819 photomultipliers.

The output pulses of each photomultiplier were amplified by two Hewlett-Packard 460A wide-band distributed amplifiers and then introduced into a coincidence circuit similar to that of Garwin.[8] The coincidence circuit was followed by pulse-shaping amplifier, stages, and then a scaler for recording the coincidences. The resolving time of the coincidence circuit was about 4×10^{-8} second.

The scintillator dimensions were 8.687 by 2.992 by 0.945 cm for the defining counter, and 11.890 by 5.951 by 2.144 cm for the rear counter for the height, width, and thickness (traversed by the counted proton) respectively. In counting, the first scintillator served to define

[7] R. L. Garwin, Rev. Sci. Instr. **23**, 755 (1952).
[8] R. L. Garwin, Rev. Sci. Instr. **21**, 569 (1950).

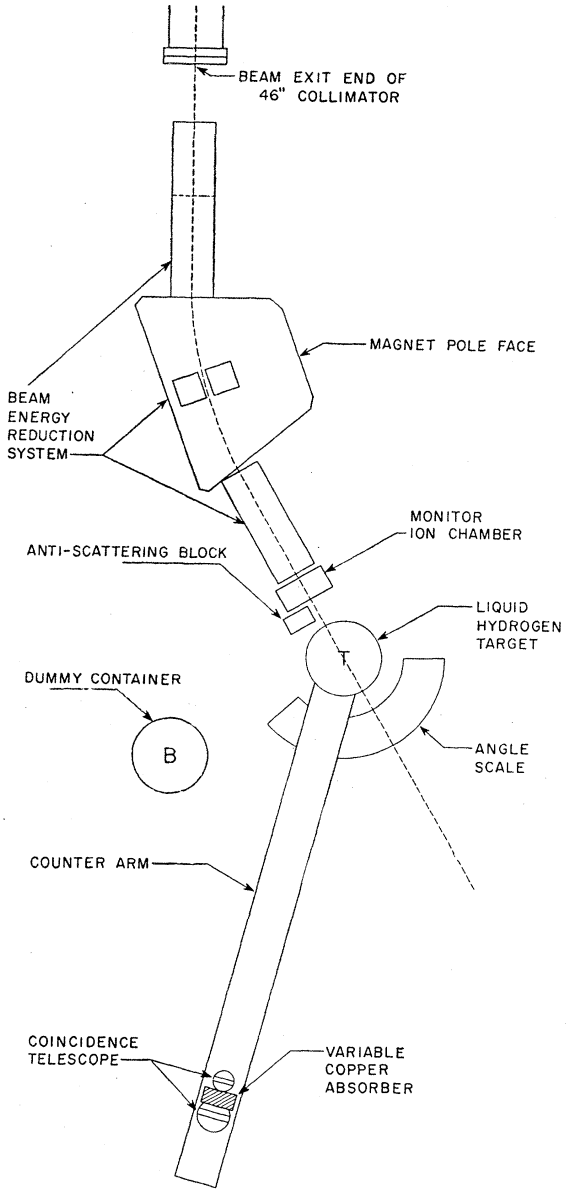

FIG. 5. Plan view of the experimental area as used for counting.

the solid angle Ω. A copper absorber, when used, was placed between the two scintillators. The rear scintillator was larger than the defining scintillator so as to make multiple-scattering losses of protons negligible. A block diagram of the counting and of the beam-calibration electronics is shown in Fig. 4.

The Beam-Calibration Equipment

Beam monitoring was done by an ion chamber which in turn was calibrated by a Faraday cup. The currents from both were integrated across capacities connected to the inputs of dc feedback electrometers. The resultant output voltage from each electrometer drove a self-calibrating Speedomax tape recorder. The features of the ion chambers and Faraday cup are given in reference 4.

The Faraday cup stops the beam in an electrically insulated brass block placed in a vacuum. The current obtained from this block should, when proper precautions are taken, be just the beam current. The number of charged particles leaving the block has been checked and is small. As is standard practice here, the Faraday cup had a magnetic field of about 100 gauss applied across the face of the 6-by-6-inch cylindrical brass block used in stopping the beam, to reduce the emission of secondary electrons. The application of $+300$ volts or -300 volts to a screen preceding the block affected the corrected Faraday current by about 1%. Consequently integration was done with the screen grounded, although the effect of screen voltage was tested during each run. This test served to indicate the number of low-energy charged particles in the vicinity of the stopping block. For good Faraday-cup vacuums, the effect of the screen voltage was always small.

III. EXPERIMENTAL PROCEDURE

Checks of Electronic Equipment

After the hydrogen target and collimating and analyzing system were aligned in the proton beam, with the aid of x-ray film, a series of checks was performed on the counting equipment. The counting arrangement is shown in Fig. 5. Coincidence counts per unit beam *versus* photomultiplier voltage were taken on each counter while the other was held constant in voltage at approximately the operating level, a plot was made, and the proper voltage setting was determined. A sample of such a voltage plateau is shown in Fig. 6. As a check on the stability of the electronic equipment, the voltage plateaus were briefly taken both at the beginning and at the end of each day's run. In each case, no change was detected. From time to time the coincidence

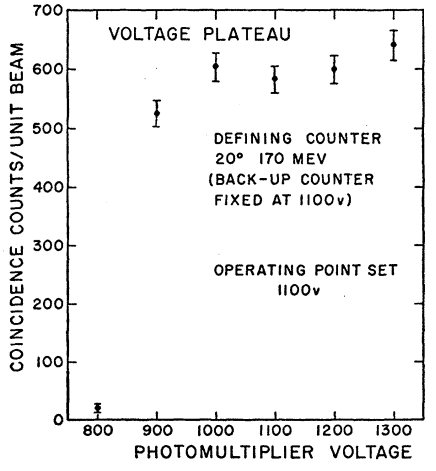

FIG. 6. A sample voltage plateau taken during Run No. 1.

circuit was checked to see that there were no coincidence counts when one or the other protomultiplier voltage was turned off. The rate of coincidences observed when the beam was turned off was never greater than two or three per minute, and would be expected to subtract out, since in general the blank coincidence counts were obtained with the same beam level as the target counts. The coincidence counting rate as a function of length of cable in each channel was measured and the cable length set for zero relative delay of the related pulses. The number of coincidence counts per unit beam was independent of beam level at all levels at which data were taken.

Determination of the Hydrogen Counts

In the subtraction of the background counts, a blank (dummy) container was used to simulate the empty hydrogen container. To be sure that the blank was sufficiently similar to the empty target, the ratio of the two was counted at various angles. The ratio was observed to be $R=0.97\pm0.02$, for all angles and absorber values (the target provided more counts).

Following the above measurements and tests of electronic equipment, the hydrogen target was filled and the determination of the number of hydrogen counts per unit beam [H in Eqs. (1) and (2a)] at one energy was started. To determine the hydrogen counts, the background counts must be subtracted. The background consisted on protons scattered from the collimator system, from the thin windows of the target, and from air traversed by the beam. Some of the background protons, especially some of those from the collimator system, were so low in energy that they could be stopped by a few grams per square centimeter of material. Since the stopping power of the full hydrogen target was greater than that of the blank, a false measure of the

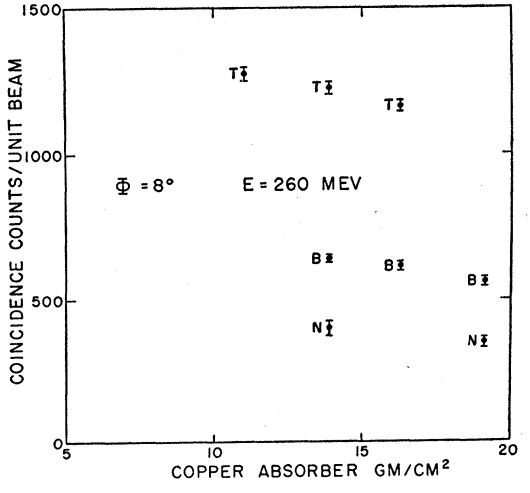

FIG. 7. Coincidence counts on target (T), blank (B), and neither (N), taken as a function of copper absorber in the counter telescope.

TABLE II. The copper equivalent of the hydrogen stopping power.

Angle (lab) (degrees)	Hydrogen path (cm)	Equivalent copper (g/cm²)
0.0	14.2	3.00±0.05
4.5	13.5	2.85±0.1
4.8–5.0	13.3	2.8 ±0.1
6.0	13.1	2.8 ±0.1
8.0	12.2	2.6 ±0.2
11.0	11.3	2.4 ±0.5
15.0	9.5	2.0 ±0.6
20.0	4.0	0.8 ±0.6
30.0	0.0	0.0 ±0.3

background was obtained if the hydrogen target was simply replaced by the blank while the remainder of the apparatus was unchanged. The false effect was small at large angles, but was very important at small angles (of the order of 10%) where the background count could be as large as the count from the hydrogen, or even larger.

Several steps were taken to insure that a proper background subtraction could be made. The first of these was the construction of the collimating and analyzing system previously described, which was quite effective in reducing the background and hence in reducing the false effect. The second was to introduce a copper absorber into the counting telescope. This reduced the background more than it reduced the effect from hydrogen, at the same time rendering the background counting rate less sensitive to the amount of material in the path of the counted particles. The third step consisted of using a slightly thicker absorber for background measurement than was used when the hydrogen target was in the beam. The additional absorber was calculated to have just the stopping power of the hydrogen in the hydrogen target. The absorbers used in the counter telescope were of the order of 15 g/cm² of copper. It was found desirable to take a series of counts per unit beam of the blank and target as a function of absorber, and to measure several differences (see Fig. 7). In this way it was possible to check the consistency of the method. There is no indication that the measured differential cross section depended on absorber at any of the angles.

To determine the stopping-power correction to the blank counts, the source of the low-energy protons that are counted on blank, but not on target, must be determined. The quantity of hydrogen that these low-energy protons traverse depends upon the angle at which they diverge from the beam and the distance of their source from the hydrogen. In the course of counting with the target and blank as a function of absorber at the various angles, a few "neither" counts, in which neither the target nor the blank container was in the beam, were included (Fig. 7). In every case, the "neither" counts reasonably paralleled those of the blank for equivalent absorber, indicating that the windows of the target (and of the ion chamber) con-

tributed very few of the low-energy protons. For the most part, these low-energy protons were scattered from the collimating system and traveled directly to the counters, or were stopped without scattering further. Using this information, and the geometry of the collimating system and target, one can determine the values of the copper equivalent in mass stopping power of the hydrogen path traversed by these protons; these values are given, together with their uncertainties, in Table II. The method is not precise, but is adequate for the magnitude of the correction. The conversion from hydrogen to equivalent copper was made by use of the tables by Aron, Hoffman, and Williams.[9]

To obtain the coincidences from hydrogen-scattered protons alone, one must subtract from the target coincidences for a given absorber value the blank coincidences corrected by the blank-to-empty ratio. The blank coincidences are to be measured at a value of counter absorber equal to the target absorber plus the copper equivalent (in stopping power) of the hydrogen traversed by the low-energy background protons. The desired blank coincidences can be obtained from the plot of blank counts as a function of absorber.

Two background checks were made during the course of the runs. The beam collimator hole was plugged by brass of thickness equivalent to several proton ranges, and coincidences were counted. With the beam collimator hole open, the scintillators were put out of line line so they could not jointly see the collimator hole, and coincidences were counted. In each case the coincidences dropped to less than 5% of the blank counts.

As a check on the defining scintillator, the whole counter was replaced by a somewhat smaller stilbene crystal, viewed by a 1P21 photomultiplier, and the counting checked at one angle. After the coincidence counts per unit beam were corrected for the difference in stopping power of the two defining counters, the ratio of the defining areas of the two counters over the ratio of their coincidence counts was 1.016 ± 0.030, indicating satisfactory agreement between different counters.

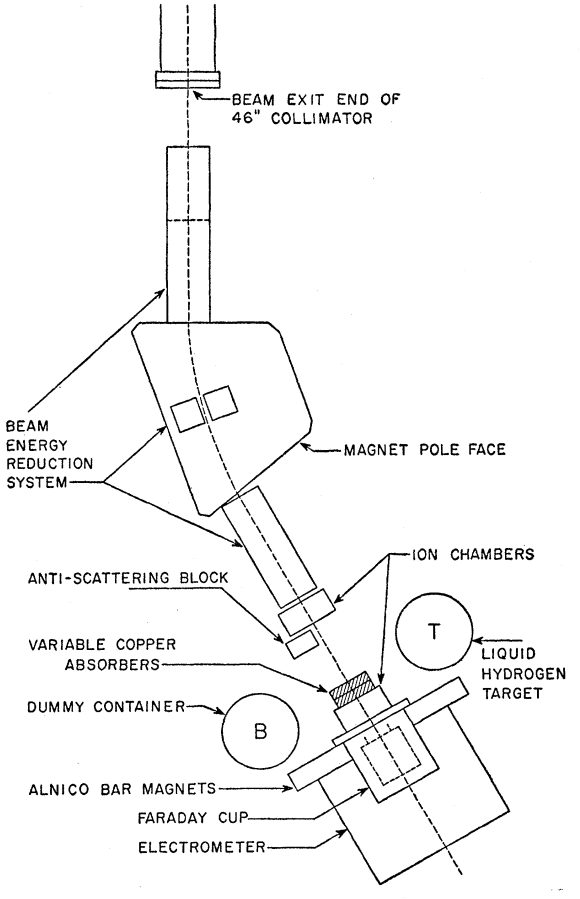

FIG. 8. Plan view of the experimental area as used for beam calibration.

[9] Aron, Hoffman, and Williams, U. S. Atomic Energy Commission Report AECU-663 (unpublished).

The Beam Calibration

The following method was devised to calibrate the monitor ion chamber (Fig. 8): With beam-collimation and monitor ion-chamber locations just as for counting, the target railroad was put on "neither" position and the Faraday cup set in place to receive the beam. The monitor ion chamber was between the last collimator slit and the antiscattering block, preceding the hydrogen target. The Faraday cup was even with the rear of the target and blank. The integrated Faraday current per unit beam was then measured as a function of absorber placed in the beam between the Faraday cup and the monitor ion chamber.

The effective multiplication M^* desired in Eq. (2a), which determines the differential cross section in the laboratory system at an angle Φ, is difficult to ascertain precisely. The following procedure has been used. The coincidence counter telescope has a cut-off energy such that only those beam protons above this energy can, upon scattering, penetrate the second counter to cause a coincidence count. This cut-off energy is determined by the variable copper absorber placed between the two counters, the energy loss from scattering into angle Φ, and the target and counter material traversed by the protons. The procedure has been to find the ratio of integrated ion-chamber current to integrated Faraday cup current for that value of copper absorber which gives the Faraday cup the same beam-energy cutoff as the counter telescope. After three corrections have been applied, the above current ratio becomes the effective multiplication M^*, and the corrected Faraday current measures only those beam protons which are capable of being counted if scattered by the target protons. Two of the corrections are such as to equate the loss of protons by nuclear collision in the Faraday cup absorber

to the nuclear loss along the path that a proton takes to count as a coincidence in the counter telescope. The third accounts for the undesirable electron contribution to the Faraday cup current arising from Coulomb scattering by beam protons in the material preceding the Faraday stopping block.

The plot of the ratio of integrated Faraday current to integrated monitor ion-chamber current as a function of absorber placed between them gives a beam range curve. When a correction for nuclear losses has been applied, the derivative of the beam range curve gives closely the distribution in range of the beam protons. One can convert the distribution in range to a distribution in energy by using the tables of Aron *et al.*[9] The above procedure was followed in obtaining the representative curve of Fig. 9, shown with the range curve from which it was derived. The nuclear loss correction has been made by use of the absorption cross sections of Kirschbaum.[10] The true distribution in energy of the beam protons is expected to be slightly narrower than the derived distribution because of the straggling in the Faraday absorber. The low-energy tails of the beam energy-distribution curves are quite inaccurately known. The initial slopes of the range curves follow closely the nuclear attenuation curve determined by the absorption cross sections of Kirschbaum. For this reason, the same angular distribution for the differential cross section can be obtained by using Kirschbaum's cross section to correct for nuclear losses, and using the Faraday cup only to obtain the ion-chamber multiplication with zero absorber. The total p-p cross section averages only about 1% lower by this method.

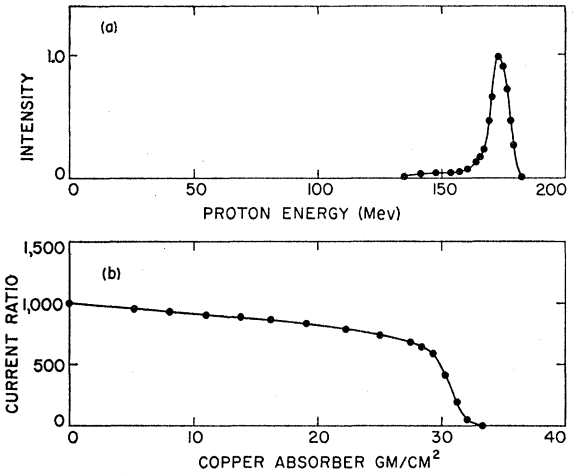

FIG. 9. (a) Sample beam-energy distribution, and (b) Faraday-cup range curve from which the beam-energy distribution was calculated. The term "current ratio" is used to indicate the ratio of Faraday-cup current to ionization-chamber current, in arbitrary units. The data were taken at 174 Mev, Run No. 2.

[10] Albert J. Kirschbaum, University of California Radiation Laboratory Report UCRL-1967, 1952 (unpublished).

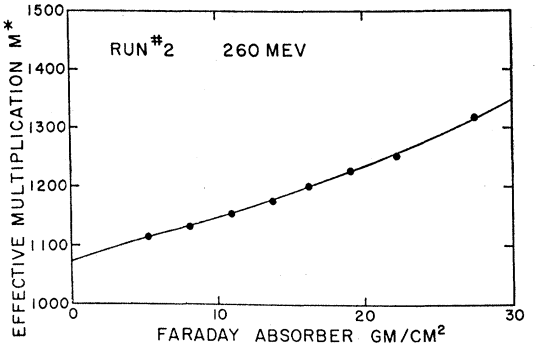

FIG. 10. A sample of the multiplication curves taken during beam calibration, for Run No. 2 at 260 Mev.

IV. CALCULATIONS AND EXPERIMENTAL RESULTS

Sample Cross-Section Calculation

The following calculation is for the laboratory angle of 8° and beam energy of 260 Mev. The data were taken during Run No. 2. The plot of counts is given in Fig. 7. To determine H, the number of protons per unit beam scattered by hydrogen, one has

$$H=T-B/R, \tag{5}$$

where T is the number of target counts per unit beam, B is the number of blank counts per unit beam, and R is the blank-to-empty ratio. For this angle and absorber value, $T=1275\pm21$, $B=645\pm14$, and $R=0.97\pm0.02$, giving $H=610\pm29$. The copper equivalent of the stopping power of hydrogen at this angle is 2.6 ± 0.2 g/cm². T is taken at 11.02 g/cm² of copper absorber, and B is for $11.02+2.6$, or 13.6 ± 0.2 g/cm² of copper absorber. The value of B is obtained from the graph (Fig. 7).

To determine the effective ion-chamber multiplication, one must first determine the cutoff energy of the counter telescope. Arbitrarily, it has been assumed that the proton must penetrate 0.1 g/cm² of the liquid scintillator in the rear counter to count a coincidence. Including this, the proton traverses material equivalent to 4.39 g/cm² of copper in mass stopping power plus the 11.02 g/cm² of the copper counter absorber, or a total of 15.41 g/cm² after scattering in the hydrogen. This range corresponds to an energy of 116 Mev. A proton with just sufficient energy to count would have this energy after scattering. The energy before scattering is 118.4 Mev, determined by use of the equation

$$E=\frac{E_s}{\cos^2\Phi[1-(E_s/2mc^2)\tan^2\Phi]}, \tag{6}$$

where E is the proton kinetic energy before scattering and E_s is the proton kinetic energy after scattering. The energy change from scattering is equivalent to that caused by 0.55 g/cm² of copper for this case. Before the proton scatters in the liquid hydrogen, it traverses, on

TABLE III. Results for Run No. 1, beam energy 170 Mev. The indicated errors are errors affecting the angular distribution alone. Estimates of the errors affecting the absolute value of the cross section are given in Table V.

Lab angle (deg)	Counter absorber (g/cm²)	T (counts/unit beam)	B (counts/unit beam)	M^*	c.m. differential cross section (mb/sterad)	Mean c.m. differential cross section (mb/sterad)	c.m. angle (deg)
	5.28	2360±30	1560±28	1354	5.84±0.42		
4.9	8.09	2153±36	1428±26	1380	5.38±0.45	5.10±0.31	10.1
	11.02	1934±31	1386±26	1431	4.09±0.42		
	5.49	1117±21	618±18	1357	3.83±0.25		
8.0	8.09	1054±19	579±18	1383	3.66±0.24	3.69±0.17	16.7
	11.02	983±16	529±18	1416	3.58±0.22		
	5.69	895±19	328±10	1358	3.63±0.18		
11.0	8.09	732±12	308±11	1383	3.35±0.13	3.52±0.11	23.0
	11.02	693±12	255± 9	1421	3.58±0.14		
	6.09	597±16	150± 9	1362	3.60±0.17		
15.0	8.09	559±12	130±13	1386	3.51±0.16	3.61±0.10	31.3
	11.02	544±12	107± 9	1431	3.71±0.15		
	0.00	675±15	212±16	1318	3.73±0.19		
20.0	2.84	601±14	164±12	1339	3.59±0.17	3.55±0.10	41.7
	5.25	529±13	134±14	1359	3.30±0.16		
	11.02	456±12	59±10	1464	3.59±0.16		
	0.00	575± 8	216±11	1314	3.20±0.14		
30.0	2.84	517±10	150± 9	1337	3.34±0.15	3.27±0.11	62.2

the average, material equivalent in stopping power to 1.72 g/cm² of copper. This includes one-half the the hydrogen and the target windows. The total of the before-scattering, scattering, and after-scattering equivalents in copper stopping power is the quantity of of copper one should place before the Faraday cup in determining the uncorrected multiplication of the ion chamber. The total is 17.68 g/cm². The multiplication curve used for this calculation, obtained with the 260-Mev beam of Run No. 2, is given in Fig. 10. For 17.68 g/cm², the uncorrected multiplication is 1212, and the three corrections previously mentioned change this to

$$M^*=1145\pm11.$$

With the use of Eq. (2b), we obtain $K=2.490\times10^{-32}$, numerically, for this calculation. From the above values for K, M^*, and H, one can obtain the laboratory cross section by use of Eq. (2a):

$$\sigma(\Phi)=KM^*H=17.42\pm0.87 \text{ millibarns per steradian.}$$

This corresponds, in the center-of-mass system, to

$$\sigma(\theta)=3.87\pm0.19 \text{ millibarns/steradian,}$$
$$\theta=17.0°,$$

obtained from Eqs. (3) and (4). The errors quoted include all estimated errors that are expected to affect the angular distribution. Generally, three cross-section measurements have been made at each angle, with a varying amount of counter absorber.

TABLE IV. Center-of-mass differential cross section $\sigma(\theta)$ at 170[a] and 260 Mev. The errors indicated are errors affecting the angular distribution alone. Estimates of the errors affecting the absolute value of the cross section are given in Table V.

Run No. 2, 174 Mev		Run No. 1, 259 Mev		Run No. 2, 260 Mev	
c.m. angle (deg)	$\sigma(\theta)$ (mb/sterad)	c.m. angle (deg)	$\sigma(\theta)$ (mb/sterad)	c.m. angle (deg)	$\sigma(\theta)$ (mb/sterad)
9.6	5.27±0.31	10.6	4.38±0.28	9.3	5.75±0.45
12.4	4.20±0.22	17.0	3.84±0.13	17.0	3.85±0.15
16.8	4.09±0.17	23.4	3.90±0.11	23.4	3.90±0.09
23.0	3.96±0.12	31.9	3.56±0.07	31.9	3.84±0.08
31.3	3.99±0.10	42.5	3.58±0.07	42.5	3.71±0.08
41.6	3.90±0.10	63.5	3.50±0.07	63.3	3.62±0.08
62.3	3.60±0.10				

[a] The results of Run No. 1 at 170 Mev are presented in more complete form in Table III.

Tabulation of Results

Table III gives the values of the center-of-mass differential cross section $\sigma(\theta)$, the angle Φ, counter absorber, T, B, M^*, and center-of-mass angle θ, for Run No. 1 at 170 Mev, as an example. The mean center-of-mass differential cross section $\sigma(\theta)$ and center-of-mass angle θ for the remaining measurements are tabulated in Table IV. The cross-section errors listed do not include absolute errors affecting only the total cross section. Table V lists estimates of the errors contributing to the uncertainty in the absolute differential cross sections. The experimental results are shown in graphical form in Figs. 11 and 12. The difference in levels of the cross sections for Run No. 1 and Run No. 2 is approximately 10% for the 170-Mev data, and 4% for the 260-Mev data; Run No. 2 is higher in each case. The source of the discrepancy is unknown.

V. CONCLUSIONS

The results of this experiment are consistent in showing the flat differential cross section in the center-of-mass system characteristic of proton-proton scattering at these energies, neglecting Coulomb effects. The total cross section is evidently rather independent of energy for the energies measured. The absolute value of the cross section is fairly well in agreement with the corresponding early results of Chamberlian, Segrè, and Wiegand, and also with their more recent work.[11] It is much lower than the original results from Rochester[12] and Harwell,[13] and somewhat higher than the level obtained at Chicago.[14]

The main reason for emphasizing the measurements at very small angles is to obtain information concerning the interference between Coulomb and nuclear scattering amplitudes. The differential scattering cross section can always be written as the sum of the terms:

$$\sigma(\theta)=\sigma_{\text{Coulomb}}(\theta)+\sigma_{\text{nuclear}}(\theta)+\sigma_{\text{interference}}(\theta).$$

The value for $\sigma_{\text{Coulomb}}(\theta)$ is well known; $\sigma_{\text{nuclear}}(\theta)$ is well known for angles greater than 35° at 170 Mev and angles greater than 28° at 260 Mev, and in each case the cross section is quite independent of angle. Since the nuclear interaction is short range, rather few l values should be involved in the nuclear scattering, so the nuclear cross section is not expected to show rapid variations with angle at the smaller angles. We wish to assume that the nuclear cross section is constant at small angles (0° to 28° or 35°). Granted this assumption, we may calculate the interference term in the cross section by subtracting from the observed cross section the known Coulomb and nuclear parts. At 170 Mev (lab) we find the interference term to be (-2.4 ± 0.6) mb/sterad at 10.1° (c.m.). At 260 Mev we find (-0.7 ± 0.4) mb/sterad at 10°. It seems doubtful that the size of the interference term should be so different at 170 Mev and 260 Mev. These results may be compared with the results of Fischer and Goldhaber[15] and of Chamberlain, Pettengill, Segrè, and Wiegand,[16] who have made measurements in the same region of angles by somewhat different methods. If analyzed along the lines outlined here, all the results seem to indicate that the interference cross section is negative, but the magnitude is not too certain.

The Coulomb scattering amplitude is known to be predominantly real and negative at the angles and energies for which the interference term has been

TABLE V. Estimates of the experimental error in the differential cross section. The table is divided so as to show separately the errors affecting the angular distribution[a] and those affecting the absolute value of cross section.

Source of error	Percent uncertainty 170 Mev	260 Mev
Errors affecting the angular distribution		
Counting statistical errors	3 to 10	2 to 10
Uncertainty in copper equivalent of hydrogen stopping power	0.5 to 2.5	0.5 to 2.5
Uncertainty in multiplication	0.5 to 2	0.5 to 2
Errors affecting the absolute value of the cross section		
Multiplication	6	4
Factors entering K [(Eq. 2(b)]	1.5	1.5
Systematic counting errors, such as slope of counter-voltage plateau and accidental coincidences	3	3
Multiple scattering in counters	0.2	0.2

[a] Estimates of the errors affecting only the angular distribution are separately indicated for each angle and energy in Tables III and IV.

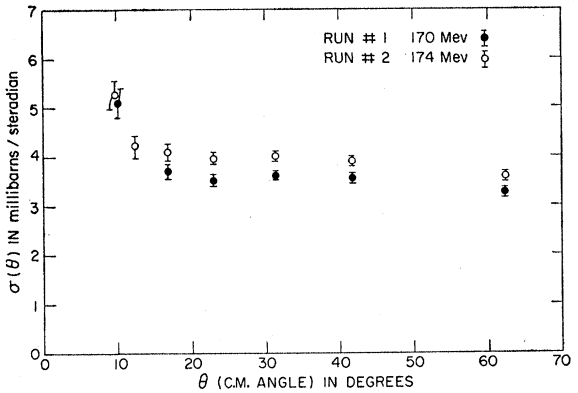

FIG. 11. The mean differential scattering cross section results in the center-of-mass system for 170 Mev. The results of Run No. 1 and Run No. 2 are given separately.

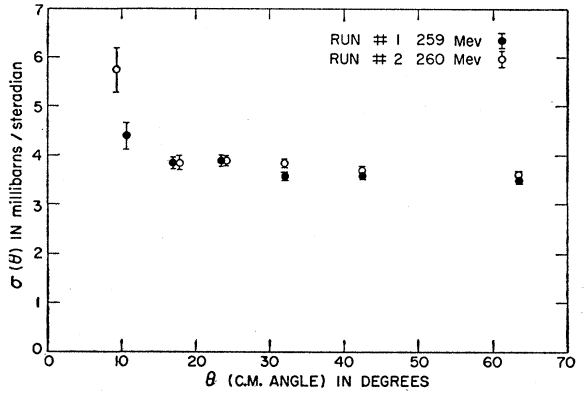

FIG. 12. The mean differential scattering cross section results in the center-of-mass system for 260 Mev. The results of Run No. 1 and Run No. 2 are given separately.

[11] Chamberlain, Pettengill, Segrè, and Wiegand, Phys. Rev. **93**, 1424 (1954).
[12] C. L. Oxley and R. D. Schamberger, Phys. Rev. **85**, 416 (1952).
[13] Cassels, Pickavance, and Stafford, Proc. Roy. Soc. (London) **A214**, 262 (1952).
[14] Marshall, Marshall, and Nedzel, Phys. Rev. **92**, 834 (1953).
[15] D. Fischer and G. Goldhaber, Phys. Rev. **95**, 1350 (1954).
[16] Chamberlain, Pettengill, Segrè, and Wiegand, Phys. Rev. **95**, 1348 (1954).

evaluated. This analysis indicates the real part of the nuclear scattering amplitude at 10° is rather small and positive.

VI. ACKNOWLEDGMENTS

Discussions with Professor Emilio Segrè and Dr. Clyde Wiegand were most helpful. The coincidence circuit was designed and built by Dr. Wiegand. It was a pleasure to work with the assistance of John A. Baldwin, Jr., David D. Clark, James W. Easley, David L. Fischer, Gordon Pettengill, Robert D. Tripp, and Francis Webb in conducting the experiment. The cyclotron crew under Jimmy Vale and Lloyd Hauser were most helpful and understanding.

PHYSICAL REVIEW VOLUME 103, NUMBER 6 SEPTEMBER 15, 1956

No-Recoil Approximations to Charged Scalar Meson Scattering

G. FELDMAN, *Institute for Advanced Study, Princeton, New Jersey*
AND
P. T. MATTHEWS, *Department of Mathematical Physics, Birmingham, England*
(Received March 2, 1956)

Feynman's method of functional integration is applied to meson-nucleon scattering. The scattering amplitude is obtained exactly in charged meson pair theory with neglect of nucleon recoil, and it is obtained in an approximation to linear charged meson theory with neglect of recoil. The results are the same as one obtains using the Chew-Low method.

1. INTRODUCTION

FEYNMAN'S[1] method of summing over histories (or functional integration) is applied to charged meson pair theory, with neglect of recoil. It appears very clearly from this approach that this interaction after mass and nucleon field normalization represents nothing but the scattering of mesons in a δ-function potential. Since the mesons are treated relativistically, they may be scattered (virtually) "backwards in time" (i.e., virtual pair creation), which gives rise to the "crossing" symmetry of the result. However, scattering is the only possible real process. These are the two typical features of scattering in a local static potential.

The method is then applied to the linear interaction in what we shall refer to as the "potential" approximation. This gives the same result as the Chew-Low[2] "one-meson" approximation.

The one-nucleon propagator and the one-nucleon–one-meson propagator, according to Feynman are, respectively,[3]

$$G(x_1,x_2)=\int G(x_1,x_2,\phi)N(\phi)\exp[I_m]\delta\phi\delta\phi^*\Big/\int N(\phi)\exp[I_m]\delta\phi\delta\phi^*, \quad (1)$$

$$\Delta(x,y;x_1,x_2)=\int G(x_1,x_2,\phi)\phi(x)\phi^*(y)N(\phi)\times\exp[I_m]\delta\phi\delta\phi^*\Big/\int N(\phi)\exp[I_m]\delta\phi\delta\phi^*, \quad (2)$$

where I_m is the uncoupled meson action, $G(x_1,x_2,\phi)$ is the one-nucleon propagator, and $N(\phi)$ is the vacuum expectation value of the S matrix in an external field ϕ. For nonrecoil theories, $N(\phi)=1$. The whole problem thus reduces to finding $G(\phi)$ and performing the functional integral, as accurately as possible.

It is clear that (2) is closely related to (1). It will be shown that the renormalized scattering amplitude can be obtained from (1) by parametric (functional) differentiation. It turns out that in order to determine the renormalized phase shift, it is only necessary to derive a formal expression for (1) for an infinite time interval. This is a special feature of no-recoil theories, which greatly simplifies the problem.

2. CHARGED PAIR THEORY

Consider the Lagrangian

$$L=\psi^*\left(i\frac{\partial}{\partial t}-m_0\right)\psi(t)-\phi^*(-\Box+\mu^2)\phi(x)-g^2\psi^*(t_x)\psi(t_x)\phi^*(x)\phi(x)\delta(\mathbf{x}). \quad (3)$$

Then $G(t,t',\phi)$ is determined by

$$\left[i\frac{\partial}{\partial t}-m_0-g^2\phi^*\phi(t)\right]G(t,t',\phi)=i\delta(t-t'). \quad (4)$$

Thus

$$G(t,t',\phi)=\theta(t-t')e^{-im_0(t-t')}\exp\left[-ig^2\int_{t'}^{t}\phi^*\phi(\tau)d\tau\right], \quad (5)$$

where $\theta(t)=1$ for $t>0$ and $\theta(t)=0$ for $t<0$.

Substituting (5) into (1) we get for the nucleon

[1] R. P. Feynman, Revs. Modern Phys. **20**, 367 (1948).
[2] G. F. Chew and F. E. Low, Phys. Rev. **101**, 1570 (1956).
[3] R. P. Feynman, Phys. Rev. **84**, 108 (1951); P. T. Matthews and A. Salam, Nuovo cimento **11**, 120 (1955).